

RSC Applied Interfaces

Accepted Manuscript

This article can be cited before page numbers have been issued, to do this please use: C. Gonsalves, J. Järvillehto, S. Saedy, J. Velasco, T. Grehl, P. Brüner, N. S. Heikkinen, J. Lehtonen, J. R. van Ommen and R. L. Puurunen, *RSC Appl. Interfaces*, 2026, DOI: 10.1039/D5LF00395D.



This is an Accepted Manuscript, which has been through the Royal Society of Chemistry peer review process and has been accepted for publication.

Accepted Manuscripts are published online shortly after acceptance, before technical editing, formatting and proof reading. Using this free service, authors can make their results available to the community, in citable form, before we publish the edited article. We will replace this Accepted Manuscript with the edited and formatted Advance Article as soon as it is available.

You can find more information about Accepted Manuscripts in the [Information for Authors](#).

Please note that technical editing may introduce minor changes to the text and/or graphics, which may alter content. The journal's standard [Terms & Conditions](#) and the [Ethical guidelines](#) still apply. In no event shall the Royal Society of Chemistry be held responsible for any errors or omissions in this Accepted Manuscript or any consequences arising from the use of any information it contains.

1 **From egg-shell to uniform distribution of platinum by atomic**
2 **layer deposition on mesoporous alumina spheres: Experiments**
3 **and modeling**

4
5 Christine Gonsalves,^{*a}, Jänis Järvillehto,^{a,b} Saeed Saedy,^b Jorge A. Velasco,^a Thomas Grehl,^c
6 Philipp Brüner,^c Niko Heikkinen,^d Juha Lehtonen,^d J. Ruud van Ommen,^b and Riikka L. Puurunen^{*a}

7 **Keywords:** *atomic layer deposition, diffusion–reaction model, porous materials*

8



^a Department of Chemical and Metallurgical Engineering, Aalto University, P.O. Box 16100, FI-00076 AALTO, Finland.

^b Department of Chemical Engineering, Process and Product Technology Institute, Delft University of Technology, Van der Maasweg 9, 2629 HZ Delft, The Netherlands.

^c IONTOF GmbH, Münster, Germany

^d VTT Technical Research Center Finland, P.O. Box 1000, FI-02044 VTT, Finland.

† Electronic supplementary information (ESI) available.

* Corresponding authors. E-mail: christine.gonsalves@aalto.fi, riikka.puurunen@aalto.fi

9 Abstract

10

11 Uniform material distribution by atomic layer deposition (ALD) inside porous materials is
12 needed in multiple applications, including batteries and catalysis. Attaining this uniformity is not
13 trivial, diffusion within the porous network being one of the main limiting factors. This work used
14 a fluidized bed atmospheric ALD reactor to coat millimeter-size mesoporous alumina spheres with
15 platinum, using the process based on (methylcyclopentadienyl)trimethylplatinum [MeCpPtMe₃]
16 and oxygen. Using different exposure times and five reaction cycles, materials with platinum load-
17 ing up to ~ 4 wt% were prepared. The growth per cycle, expressed as average areal number density,
18 was approximately 0.1 Pt atoms/nm². Cross-sectional analysis done using low-energy ion scatter-
19 ing indicated that with increasing exposure time, platinum distribution evolved from egg-shell to
20 macroscopic uniform distribution through the particles. Diffusion–reaction modeling was done to
21 support the experiments and showed a saturation of the Pt weight loading after uniform distribution.
22 This work shows that it is possible to get a uniform distribution of platinum through mesoporous
23 particles with an aspect ratio on the order of 100,000:1, when the ALD process is properly opti-
24 mized.

25 1 Introduction

26 Atomic layer deposition (ALD) is a technique that is based on sequential and self-limiting gas-solid
27 surface reactions^{1,2}, widely used for fabricating uniform thin films on flat substrates and confor-
28 mal coatings in complex, high-aspect-ratio structures^{1,3}. In principle, ALD can enable conformal
29 growth on any surface, regardless of geometry, since the reactions occur by chemisorption. Over
30 a thousand ALD chemistries have been developed, reflecting its broad application potential^{4,5}.
31 ALD is attractive for coating particles,^{3,6–8} with growing applications in heterogeneous thermo-
32 catalysis^{9,10}, battery electrodes¹¹, fuel cells¹², LED phosphors^{13,14} and drug delivery systems¹⁵.
33 Recently, a review article overviewed ~800 scientific articles reporting ALD on particulate mate-
34 rials¹⁶.

35 ALD is attractive for coating porous materials with expensive noble metals such as platinum,
36 as it potentially provides precise particle size control and efficient use of precursors¹⁷. Platinum is



37 a critical catalyst in applications such as fuel cells^{12,18,19}, where it facilitates the oxygen reduction
38 and hydrogen oxidation reactions²⁰, and in hydrogenation processes^{21,22}, where it activates molec-
39 ular hydrogen. Deposition of platinum by ALD has been demonstrated on a variety of substrates,
40 including nonporous anodic alumina membranes^{23–27} and porous nanotubes^{28–30}, and trench-type
41 high-aspect-ratio geometries^{31–34}. Platinum ALD has been reported to date^{4,5,16} using a handful of
42 precursors: platinum(II) acetylacetonate [Pt(acac)₂]³⁵, dimethyl(η^4 -cyclohexa-1,5-diene)platinum
43 [PtMe₂(η^4 -cyclohexa-1,5-diene)]³⁶, dimethyl(*N,N*-dimethyl-3-butene-1-amine-*N*)platinum (DDAP,
44 [C₈H₁₉NPt])^{37,38}, and (methylcyclopentadienyl)trimethylplatinum [MeCpPtMe₃]^{39–43}. Out of these,
45 MeCpPtMe₃ is the most commonly used Pt precursor due to its stability and high volatility^{16,32},
46 and has been used in this work.

47 Several experimental studies have investigated the macroscopic distribution of various ALD-
48 deposited materials on porous substrates. Table 1 summarizes earlier work on porous spheres.
49 While most studies^{44–46} report only an eggshell-type coating, there are also reports where uniform
50 coating (i.e., through particle coating) is seen^{47–49}. Elam *et al.*⁴⁷ showed that progressively increas-
51 ing the exposure (partial pressure \times time) led to increasing penetration upto uniform coating for a
52 Al(CH₃)₃/H₂O ALD process with a 90 s precursor exposure time in porous silica particles (aspect
53 ratio 1667:1, calculated as the ratio of particle radius to average pore diameter). To date, the highest
54 aspect ratio for which uniform coating on a porous sphere has been reported is 43103:1, done using
55 a Ru(EtCp₂)/O₂ ALD process on alumina spheres with a 180 s precursor exposure time⁴⁸.

56 To better understand and predict film conformality in challenging geometries, various models
57 including analytical⁵⁰, diffusion–reaction^{51–54}, ballistic transport–reaction^{53,55}, and Monte-Carlo³
58 models have been developed to describe ALD growth in trenches, holes, and porous materials. For
59 example, the analytical Gordon *et al.* model⁵⁰ showed that the penetration depth within a hole
60 for Knudsen diffusion conditions (i.e. Knudsen number \gg 1, where Knudsen number is the ratio
61 of the gas mean free path to a characteristic length scale) is proportional to the square root of the
62 precursor exposure time⁵⁰. Recently, a diffusion–reaction model⁵⁶ was adapted for porous particles
63 in the shape of slabs, cylinders and spheres, where reactant transport initiates at the particle’s outer
64 surface and proceeds through a tortuous pathway toward the center, with the effective diffusion
65 coefficient governing diffusion throughout the particle⁵⁶. This model shows that spherical particles



66 require less reactant exposure for full surface saturation than slabs or cylinders of the same size due
67 to multidimensional reactant diffusion propagation along three radial directions (spheres require
68 about one-third of the exposure required to saturate slabs)^{56,57}.

69 The goal of this work is to characterize ALD growth of platinum on mesoporous alumina
70 spheres in a fluidized bed reactor at atmospheric pressure using the commonly used
71 (trimethyl)methylcyclopentadienylplatinum(IV) reactant. We show that systematically increasing
72 precursor exposure leads to increasing Pt penetration depth, from egg-shell to uniform distribu-
73 tion; on porous spheres up to 2.5 mm diameter with an aspect ratio on the order of 100,000 : 1.
74 These experimental results are then compared with predictions from a diffusion—reaction model
75 for spheres⁵⁶. The model predictions align with the experiments, assuming a low precursor sticking
76 coefficient.



77 2 Methods

78 2.1 Materials

79 Porous alumina spheres from SASOL Limited were used as the ALD support. The diameters
80 were 1.0 mm (Alumina Spheres 1.0/160 prod. 610110), 1.8 mm (Alumina Spheres 1.8/210, prod.
81 604130) and 2.5 mm (Alumina Spheres 2.5/210 prod. 608114). The reactants used were:
82 (Trimethyl)methylcyclopentadienylplatinum(IV), MeCpPtMe₃ (99%) from Strem Chemicals Inc.,
83 and synthetic air (Linde) Nitrogen (N₂, 99.999%, Linde) was used as the inert carrier gas.

84 2.2 Platinum ALD

85 Platinum ALD was done at atmospheric pressure in a fluidized bed reactor with a process tem-
86 perature of 110 °C. The fluidized-bed ALD reactor used in this study has been described in detail
87 elsewhere^{60,61}; a schematic is provided in the supporting information (Figure S2). The process con-
88 ditions were similar to those reported by Grillo et al.⁶⁰. The Pt precursor was placed in a stainless
89 steel bubbler and was heated to 70 °C. The process consisted of the steps: MeCpPtMe₃ exposure
90 (duration from 180 s to 1440 s), purge I (600 s), synthetic air exposure (600 s), purge II (600 s).
91 Parameters varied during the experiments are in Table 2. The alumina spheres were mixed with
92 glass beads of 120 – 150 μm diameter. Each run used 10 grams of glass beads and 0.25 grams of
93 alumina spheres for each diameter of 1.0 mm, 1.8 mm, and 2.5 mm. Given that the particle mixing
94 time in the fluidized bed (~1 s) is significantly shorter than the precursor pulse time, each particle is
95 expected to experience a uniform time-averaged concentration, promoting a homogeneous coating
96 across the batch.^{16,62,63} In the experiments conducted, a flow rate of 1 l min⁻¹ (normal liter per sec-
97 ond at 1 atm and 20 °C) was used, resulting in a fluidization velocity of approximately 3.4 cm s⁻¹.
98 Detailed conditions for fluidization are in the supporting information (Section S1.4).

99 Before ALD, the glass beads for the sample mixture were washed with diluted isopropanol
100 (~20 %), and after that, with diluted nitric acid (~10 %). Four samples of Pt/Al₂O₃ were obtained
101 by varying the MeCpPtMe₃ pulse time (180, 360, 720, and 1440 s) while the oxidizer's pulse time
102 was kept constant at 600 s; five cycles of ALD were done for all samples.



Table 2 Varied flows used in the experimental setup (total flow was constant: 1 l min⁻¹). One cycle consisted of the following steps: MeCpPtMe₃ exposure, purge I, synthetic air exposure, purge II.

Step	$\dot{V}_{N_2, \text{purgeI}}^1$ L/min	$\dot{V}_{N_2, \text{bubbler}}^2$ L/min	$\dot{V}_{N_2, \text{purgeII}}^3$ L/min	$\dot{V}_{N_2, \text{makeup}}^4$ L/min	\dot{V}_{air}^5 L/min
MeCpPtMe ₃ exposure	0	0.4	0	0.6	0
Purge I	0.8	0	0	0.2	0
Synthetic air exposure	0	0	0	0	1
Purge II	0	0	0.8	0.2	0

1 $\dot{V}_{N_2, \text{purgeI}}$ is the nitrogen volume flow bypassing the MeCpPtMe₃ bubbler

2 $\dot{V}_{N_2, \text{bubbler}}$ is the nitrogen volume flow through the MeCpPtMe₃ bubbler

3 $\dot{V}_{N_2, \text{purgeII}}$ is the nitrogen volume flow through the air line

4 $\dot{V}_{N_2, \text{makeup}}$ is the nitrogen makeup volume flow

5 \dot{V}_{air} is the air volume flow

103 2.3 Nitrogen physisorption

104 The surface area, total pore volume, and pore size of the spheres was determined by nitrogen
105 physisorption. The measurements were made with a Micromeritics Tristar II 3020 instrument.
106 The specific surface area was determined using the Brunauer–Emmett–Teller (BET)⁶⁴ method.
107 Total pore volume and the pore size distribution were determined by the Barrett–Joyner–Halenda
108 (BJH)⁶⁵ method.

109 2.4 Inductively Coupled Plasma-optical emission spectrometry

110 The average metal weight loading of platinum on the porous alumina spheres was determined using
111 a PerkinElmer Optima 8000 inductively coupled plasma-optical emission spectrometer. In the
112 inductively coupled plasma-optical emission spectrometry (ICP-OES) analysis, each particle size
113 fraction was analyzed separately. Approximately 30 mg of the sample was digested in a microwave
114 for 60 minutes in a mixture of 4.5 ml of 30% hydrochloric acid and 1.5 ml of 65% nitric acid. The
115 samples were then diluted to 50 ml with purified water before the analysis with ICP-OES 8000.

116 2.5 Average areal number density calculation

117 From experimental values of average metal weight loadings (in this work determined from ICP-
118 OES), the average number of metal atoms per surface area of the support, referred to as areal



119 number density $c_M(\text{nm}^{-2})$ is calculated as²⁸

$$c_M = \frac{w_M N_0 m_t}{M_M S m_s}. \quad (1)$$

120 Here, w_M is the weight fraction of the metal, N_0 (mol^{-1}) is Avogadro's constant, M_M ($\text{g}_{\text{metal}} \text{mol}^{-1}$)
121 is the molar mass of the metal, S ($\text{m}^2 \text{g}_{\text{support}}^{-1}$) is the specific surface area of the support, m_t (g_{sample})
122 is the total mass of the sample including the amount of the deposited material, and m_s ($\text{g}_{\text{support}}$) is
123 the mass of the original support. An example of the average areal number density calculation is in
124 Section S2.2 of the supporting information. Additionally, for the largest sphere size (2.5 mm), we
125 calculated the areal number density on the coated area, based on the coated volume fraction ϕ_{coat}
126 (Table S2 in the supporting information).

127 2.6 CO pulsed chemisorption

128 CO pulsed chemisorption was used to analyse platinum crystallite size and dispersion of ALD
129 coated Pt/Al₂O₃ spheres of diameter 2.5 mm. An AutoChem-III 2930 tool (Micromeritics Instru-
130 ment Corporation) with an external CirrusTM 3 mass spectrometer (MS; MKS Instruments) was
131 used.

132 In a U-shaped reactor tube, approximately 60 mg of sample was placed and diluted with 300
133 mg of silicon carbide, SiC (Thermo Scientific, 46 grit). The sample was then dried by heating to
134 200 °C (ramp rate: 10 °C/min) for 1 hour in a helium (He, Woikoski, 99.9995%) flow of 50 ml/min
135 and then cooled to 35 °C after drying. Flow was then changed from He to a gas mixture of H₂/Ar
136 (10% H₂ in Ar, Air products, 9.99%) with a flow rate of 50 ml/min. The sample was then reduced
137 in a gas mixture of H₂/Ar while heating to 400 °C (ramp rate: 10 °C/min). The hold time at 400
138 °C was 0.5 hour. After reduction, flow was changed to He to remove chemisorbed hydrogen (flow
139 rate 50 ml/min), and after 0.5 hour, the sample was cooled to 35 °C.

140 Then, pulse chemisorption of CO was carried out. In total, 25 pulses of CO/He (10% CO in
141 He, Air products, 9.998%) were dosed to the sample using a loop. The physically calibrated loop
142 volume was 0.5185 cm³. The temperature of the loop and the equipment's lines was 110 °C. The
143 thermal conductivity detector (TCD) and mass spectrometer, $m/z = 28$ (CO) signals were used
144 to estimate the amount of CO adsorbed. Pt dispersion and platinum crystallite particle size were



145 calculated based on the CO consumption, assuming hemispherical Pt particles and an adsorption
146 stoichiometry of 1. The equations used to calculate metal dispersion and hemispherical crystallite
147 size are provided in the supporting information (Section S1.3).

148 **2.7 Low-energy ion scattering**

149 Low-energy ion scattering (LEIS) surface spectroscopy was performed on the inner surfaces of the
150 samples using an IONTOF Qtac 100 low-energy ion scattering spectrometer. The purpose was to
151 study the propagation of the ALD Pt coating from the outer surface towards the center of the porous
152 alumina spheres. Before analysis, the spheres were mechanically cut approximately in half with
153 scissors to obtain cross-sections, and the samples were cleaned in the ultra-high vacuum of the
154 instrument by exposure to atomic oxygen extracted from a remote plasma source. $^4\text{He}^+$ was used
155 as the analysis ion (3 keV, 5.2 nA) with an acquisition time of 1200 s, scanning over an analysis
156 area of $2.8 \times 2.8 \text{ mm}^2$ using a 256×256 pixel raster. The resulting ion dose density was 4.8×10^{14}
157 ions/cm². The PtO₂ surface coverage was quantified via a PtO₂ powder reference sample (Sigma
158 Aldrich, CAS: 1314-15-4). The horizontal line scans through the center of the alumina spheres
159 are averaged over 16 pixels in the vertical direction. Line scans are plotted with 11 pt adjacent
160 averaging.

161 **2.8 Diffusion–reaction Model**

162 A diffusion–reaction model was used to compare the saturation profiles obtained experimentally
163 with those predicted by simulations. The model equations are based on the diffusion–reaction
164 model for porous spheres by Heikkinen et al.⁵⁶ and the model by Ylilammi et al.^{51,52} The main
165 equations are described in this section, and some additional equations are shown in the supporting
166 information (Section S1.1). The set of equations was solved using a Python-based script.⁶⁶ This
167 model assumes uniform porosity, tortuosity, and pore size across the entire particle. It takes the
168 precursor partial pressure at the entrance p_{A0} (related to the reactant number density n_{A0} through
169 the ideal gas equation) as a constant value, and describes reactant transport through diffusion from
170 the outer surface towards the core of a sphere of radius R :



$$\frac{\partial n_A(r,t)}{\partial t} = D_{eff} \frac{\partial^2 n_A(r,t)}{\partial r^2} + D_{eff} \frac{2}{r} \frac{\partial n_A(r,t)}{\partial r} - \bar{s} \cdot \left[\frac{1}{4} \bar{v}_A \cdot c \cdot n_A(r,t) \cdot [1 - \theta(r,t)] - P_d \cdot q \cdot \theta(r,t) \right] \quad (2)$$

171 and rate of change of surface coverage:

$$\frac{\partial \theta(r,t)}{\partial t} = \left[\frac{1}{4q} \bar{v}_A \cdot c \cdot n_A(r,t) \cdot [1 - \theta(r,t)] - P_d \cdot \theta(r,t) \right]. \quad (3)$$

172 Here, n_A (m^{-3}) is volumetric reactant A number density (related to the partial pressure of the
173 reactant p_A through the ideal gas equation), D_{eff} ($\text{m}^2 \text{s}^{-1}$) is the effective diffusion coefficient, θ (-)
174 is surface coverage, \bar{s} (-) is the ratio of specific surface area (S) ($\text{m}^2 \text{g}^{-1}$), and pore volume (V_{pore})
175 ($\text{m}^3 \text{g}^{-1}$), \bar{v}_A (m s^{-1}) is the mean thermal velocity, q (m^{-2}) is the adsorption capacity, c (-) is the
176 sticking coefficient, and P_d (s^{-1}) is the desorption probability.

177 The effective diffusion coefficient D_{eff} in Equation 2 is calculated as^{56,67}

$$D_{eff} = \frac{\varepsilon}{\tau} \cdot \left(\frac{1}{\frac{1}{D_A} + \frac{1}{D_{Kn}}} \right). \quad (4)$$

178 Here, D_A ($\text{m}^2 \text{s}^{-1}$) is the molecular diffusion coefficient, which describes gas phase collisions
179 (molecule–molecule interactions), and the D_{Kn} ($\text{m}^2 \text{s}^{-1}$) is the Knudsen diffusion coefficient which
180 dominates at low pressures and describes molecule-wall interactions. Porosity, ε (unitless) of the
181 spheres is calculated using the relation⁶⁸:

$$\varepsilon = \frac{V_{pore}}{V_{pore} + \frac{1}{\rho_s}}. \quad (5)$$

182 In Equation 5, V_{pore} ($\text{cm}^3 \text{g}^{-1}$) is the pore volume, and ρ_s (g cm^{-3}) is the skeletal density of the
183 support material γ -alumina, 3.6 g cm^{-3} ⁶⁹. Tortuosity τ (unitless) is calculated from the Beekman
184 relationship for heterogeneous catalysts as follows^{70,71}:

$$\tau^2 = \frac{\varepsilon}{1 - (1 - \varepsilon)^{1/3}}. \quad (6)$$



185 The weight percentage of the metal for a partly coated particle can be calculated by

$$w_M = \frac{q \times M_M \times S \times m_S}{N_0 \times m_t} \phi_{\text{coat}}, \quad (7)$$

186 where M_M (g mol^{-1}) is the molar mass of the metal, S ($\text{m}^2 \text{g}^{-1}$) is the specific surface area of the
 187 support, m_S (g) is the mass of the support, N_0 is Avogadro's constant, m_t (g) is the total particle
 188 mass, and ϕ_{coat} (-) is the coated volume fraction of the porous sphere. The ϕ_{coat} is obtained from
 189 integration of the simulated saturation profile $\theta(t_{\text{final}}, r)$ as a function of $1 - (r/R)^3$. For a fully
 190 coated porous sphere, ϕ_{coat} is one. In the case of a step-like saturation profile with a penetration
 191 depth d , the coated volume fraction is equivalent to^{6,72}

$$\phi_{\text{coat}} = \frac{V_d}{V_R} = \frac{(R^3 - (R-d)^3)}{R^3}, \quad (8)$$

192 where V_d is the coated volume, and V_R is the total internal volume of the sphere. A simplified figure
 193 showing the coated volume fraction is in the supporting information (Figure S1).

194 3 Results

195 3.1 Support characterization

196 Support surface characteristics were studied by nitrogen physisorption. The average specific sur-
 197 face area, pore volume, and pore diameter values for the spheres of different diameters and the
 198 resulting aspect ratios are in Table 3. All alumina supports were mesoporous with an average
 199 pore diameter from 9.9 to 11.7 nm and a narrow pore size distribution (Figures S3 and S4 in the
 200 supporting information).

201 3.2 Quantification of Metal Weight Loading: ICP-OES

202 After Pt ALD using reactants MeCpPtMe₃ and synthetic air, the average metal weight loading on
 203 spherical alumina was determined by ICP-OES. Results for weight loadings on spheres of different
 204 diameters are presented in Figure 1a and platinum loading in terms of the average areal number
 205 density, i.e, metal atoms per support surface area, is in Figure 1b. For spheres of all sizes, the



Table 3 Nitrogen physisorption results: BET surface area, total pore volume, median pore radius. Calculated aspect ratio^a, porosity^b, and tortuosity^c values are also included.

Sphere diameter (mm)	BET surface area, S ($\text{m}^2 \text{g}^{-1}$)	Pore volume, V_{pore} ($\text{cm}^3 \text{g}^{-1}$)	Average pore diameter, d_{pore} (nm)	Aspect ratio ^a (-)	Porosity ^b ϵ (-)	Tortuosity ^c τ (-)
1.0	158	0.49	11.7	42700: 1	0.64	1.49
1.8	202	0.55	10.3	87300: 1	0.67	1.47
2.5	206	0.54	9.9	126000: 1	0.66	1.48

^a Aspect ratio is calculated as the ratio of particle radius R to average pore diameter d_{pore} .

^b Porosity ϵ (-) is calculated using pore volume V_{pore} ($\text{cm}^3 \text{g}^{-1}$) and the skeletal density of γ -alumina, ρ_{S} (3.6 g cm^{-3})⁶⁹ described in Equation 5.

^{c2} Tortuosity τ is calculated from the porosity using Equation 6.

206 average platinum weight loading increased with exposure time, though a slower increase was seen
 207 for the longest exposure time (1440 s). Up to 4.05 Pt wt% metal loading was observed, for sphere
 208 with a diameter of 1.8 mm (surface area = $202 \text{ m}^2/\text{g}$) at the longest exposure time (1440 s). As
 209 seen in Figure 1b, the maximum average areal number density after five cycles of about 0.71 Pt
 210 atoms/ nm^2 was observed for the sphere size 1.0 mm with the highest exposure time (1440 s), with
 211 all sphere sizes showing a close value.

212 3.3 CO pulse chemisorption

213 Results from CO pulse chemisorption are presented in Table 4. As the ALD exposure time of the
 214 MeCpPtMe₃ reactant increased from 180 s to 1440 s, the cumulative quantity of CO chemisorbed
 215 on the surface initially increased and then settled. The CO adsorption capacity of the samples varied
 216 from $65 \mu\text{mol/g}$ for the shortest exposure to $118 \mu\text{mol/g}$ for the longest exposure. For the shortest
 217 exposure time, the number of CO molecules chemisorbed exceeds the number of platinum atoms
 218 on the surface (by ICP-OES), likely indicating an adsorption mode where one platinum atom can
 219 bind to more than one CO molecule. The dispersion calculation assumes the bonding of one CO per
 220 platinum atom (Supporting information, Section S1.3). While for the shortest exposure time, the
 221 dispersion cannot be calculated with this assumption (it is very high, presumably $\sim 100\%$), for the
 222 other exposure times, the calculated dispersion varies from 84% to 41%, and dispersion decreases
 223 with exposure time. The particle size calculated assuming hemispherical particles at the same time
 224 increases from 1.3 to 2.8 nm.



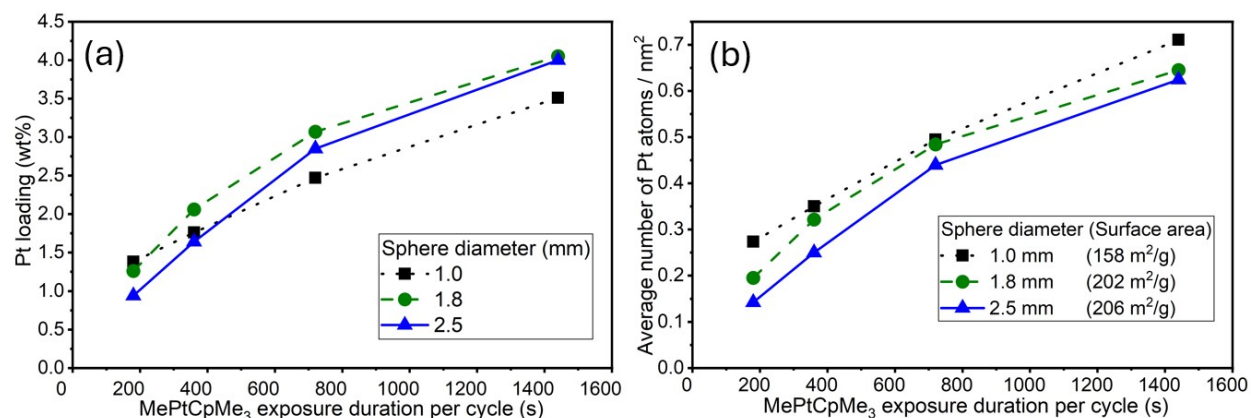


Figure 1 (a) Platinum loading (wt%) and (b) average platinum areal number density (atoms/nm²) as a function of the MeCpPtMe₃ exposure time (exposure time per cycle), based on ICP-OES and surface area of the support as in Table 3. Five ALD cycles were done at a reaction temperature of 110 °C, in a fluidized bed at atmospheric pressure. Numerical values corresponding to this figure are in Table S1 of the supporting information.

Table 4 Characterization results from CO pulse chemisorption (TCD measurements) done on Pt-coated alumina spheres of diameter 2.5 mm^a.

MeCpPtMe ₃ exposure time (s)	Cumulative CO quantity (cm ³) (STP)	Cumulative CO quantity (μ mol/g)	Cumulative quantity (CO molecules /nm ²)	ICP-OES weight loading (%) for 2.5 mm sphere	Average areal number density (Pt atoms/nm ²)	Metal dispersion	Crystallite size (hemisphere) (nm)
180	1.46	65.2	0.19	0.94	0.14	_b	_b
360	1.59	70.7	0.21	1.64	0.25	84.1%	1.3
720	2.67	119.1	0.35	2.85	0.44	81.5%	1.4
1440	2.65	118.4	0.35	4.00	0.62	57.7%	2.0

^a Mass spectrometer results are in Table S3 of the supporting information.

^b The cumulative quantity of CO chemisorbed exceeded the number of Pt atoms, and dispersion can be assumed to be approximately 100%. The stoichiometry of adsorption may differ from the stoichiometry value of one, assumed in the dispersion and crystallite size calculations.



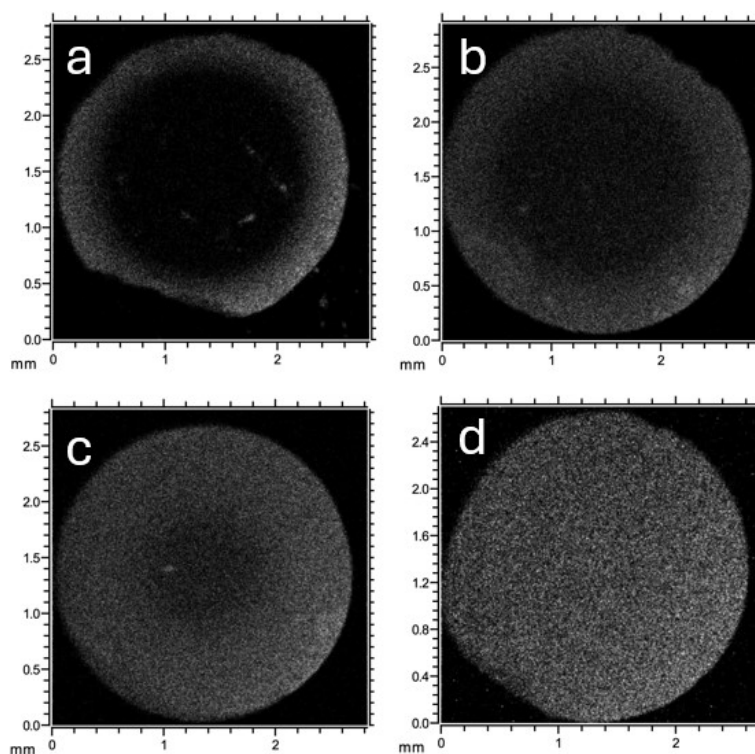


Figure 2 Low-energy ion scattering (LEIS) qualitative maps showing platinum surface across cross-sections of 2.5 mm (diameter) ALD coated Pt/Al₂O₃ spheres. Brighter areas indicate higher surface coverage of platinum. The platinum reactant exposure time per cycle was (a) 180 s, (b) 360 s, (c) 720 s, and (d) 1440 s.

225 3.4 Surface chemical composition analysis: LEIS

226 LEIS reveals the presence of Pt, Al and O on the surface (example spectra in the supporting in-
227 formation, Figure S5). Figure 2 shows distribution maps of PtO₂ by LEIS and Figure 3 gives the
228 quantified results for the PtO₂ signal through the particle. Overall, the Pt penetration increased
229 with increasing exposure time. An egg-shell coating is seen in samples with lower exposure times
230 of 180, 360 and 720 s. For the sample with the longest exposure time of 1440 s, the coating ap-
231 peared to be macroscopically uniform throughout the sample. The corresponding surface fraction
232 of PtO₂ was approximately 5%. Considering that an average monolayer of PtO₂ has about 9.9 Pt
233 atoms/nm² (calculated from the bulk density $\rho = 11.8 \text{ g/cm}^3$, and molar mass = 227.08 g/mol of
234 PtO₂), the LEIS results correspond to a surface areal number density of about 0.5 Pt atoms/nm².



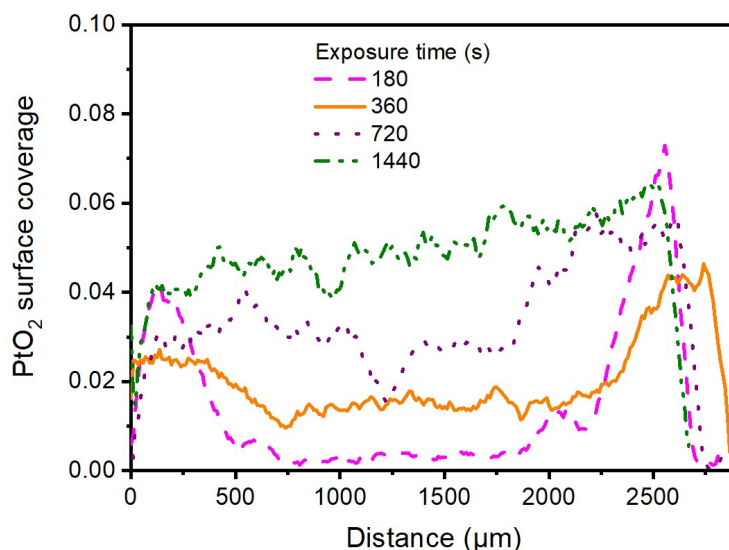


Figure 3 Quantified line scans of the LEIS images in Figure 2 for ALD coated Pt/Al₂O₃ spheres (diameter: 2.5 μm). The horizontal line scans through the center of the alumina spheres are averaged over 16 pixels in the vertical direction and are plotted with 11-point adjacent averaging.

235 3.5 Diffusion–reaction simulations

236 Diffusion–reaction simulations were made to support the experimental study. The modeling was
 237 made assuming ideal ALD, i.e., saturating and irreversible adsorption steps, although the model
 238 would allow reversibility as well. Realistic parameters were chosen that are related to the ALD
 239 process conditions; the parameters are listed in the caption of Figure 4. To have a resemblance
 240 between simulations and experiments, the partial pressure of the platinum reactant and the sticking
 241 coefficient were varied (the average areal number density of platinum was assumed as 0.12 nm⁻²).
 242 To have results similar to LEIS (and X-ray photoelectron spectroscopy, see supporting information
 243 section S2.6) that show through-penetration (uniform macroscopic distribution) for the exposure
 244 times of 1440 s, the sticking coefficient had to be made very small, on the order of 10⁻⁹.

245 4 Discussion

246 4.1 Comparison of Pt loading to literature values

247 The Pt metal loading observed in this study is consistent with values for platinum reported in the
 248 literature for ALD on particulate materials. To enable comparison with literature, the average areal



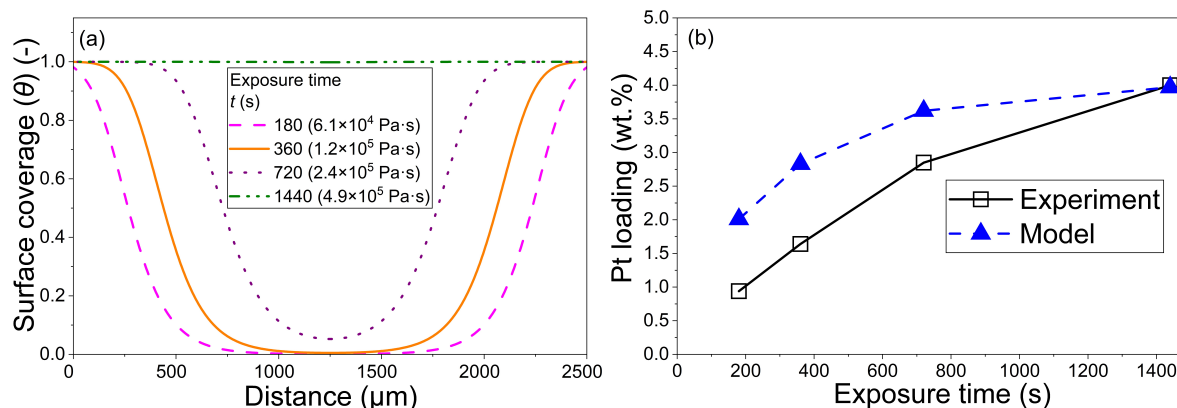


Figure 4 (a) Simulated surface coverage profiles, along the radial direction from the outer surface towards the center and back, along the radius of a 2.5 mm alumina sphere. (b) Comparison of the average Pt weight loading from the model to the experiments (ICP-OES results in Figure 1). The sticking coefficient used for the simulation was 10^{-9} . Corresponding pressure profiles are shown in the supporting information (Figure S8). Other parameters were: Reactant was MeCpPtMe_3 ; particle diameter = 2.5 mm ($R = 0.00125$ m); $\varepsilon = 0.66$; $\tau = 1.5$; $d_{\text{pore}} = 9.9$ nm; $S = 206$ m² g⁻¹; $V_{\text{pore}} = 5.4 \times 10^{-7}$ m³ g⁻¹; $\rho_S = 3600$ kg m⁻³; $q = 0.12$ nm⁻²; $P_d = 0$ s⁻¹; $T = 383$ K; $p_{A0} = 340$ Pa; $p_I = 99660$ Pa; the molar mass of reactant M_A : 0.319 kg mol⁻¹; the molar mass of inert M_I : 0.028 kg mol⁻¹; $d_A = 8.13 \times 10^{-10}$ m; $d_I = 3.74 \times 10^{-10}$ m; $M_M = 0.195$ kg mol⁻¹. The calculated Kn number was ~ 1.4 (transition region) and the Thiele modulus was ~ 12 (diffusion-limited process), see supporting information section S1.2.



249 number density was calculated from the reported values of Pt weight loading. In this work, the
250 weight loading for the longest exposure time (1440 s) ranged from 3.5 wt% for 1.0 mm sphere
251 to 4 wt% for the 2.5 mm sphere (Figure 1). These weight loadings translate to growth per cycle
252 (GPC) in terms of average areal number density of 0.71 and 0.62 atoms/nm² after five cycles, or
253 ~ 0.14 and 0.12 Pt atoms/nm² per cycle for the sphere sizes 1.0 and 2.5 mm, respectively (Table
254 S1). The GPC of 0.14 and 0.12 Pt atoms/nm² corresponds to approximately 1% of an average Pt
255 monolayer, calculated from the bulk density and mass of Pt (see Eq. 16 in ref.⁷³, $\rho = 21.45$ g/cm³,
256 areal number density of an average platinum monolayer $c_M^{ml} \approx 16.4$ atoms/nm²).

257 The values of average areal number density estimated from the literature data vary over a broad
258 range. For example, with MeCpPtMe₃ on mesoporous silica gel at 325 °C, the Pt loading cor-
259 responds to an average areal number density of 0.03 atoms/nm² per cycle (over three cycles)⁵⁹.
260 For another study with MeCpPtMe₃ on graphene nanoplatelets at 100°C the average areal num-
261 ber density corresponds to 0.13 atoms/nm² per cycle (over 10 cycles)⁷⁴ and on carbon black at
262 300°C corresponds to 0.16 atoms/nm² per cycle (over 15 cycles)⁷⁵. On other types of carbon sup-
263 ports, even higher average areal number density values were also observed. For example in the
264 case of MeCpPtMe₃ on multi-walled carbon nanotubes^{30,76} at 300°C (one cycle), average areal
265 number density corresponds to 0.49 atoms/nm² and on carbon (Vulcan XC72R) at 300°C for fuel
266 cells⁷⁷, average areal number density corresponds to 2.2 atoms/nm² per cycle (over five cycles).
267 Overall, the literature range for Pt average areal number density is broad, from 0.03⁵⁹ up to 2.2⁷⁷
268 atoms/nm² per cycle. The average areal number density results of this work, values between 0.14
269 to 0.12 Pt atoms/nm² per cycle fall well within the range observed in previous literature.

270 4.2 Choice of a low sticking coefficient for simulations

271 For simulations, a resemblance with experimental saturation profile data can be achieved only with
272 the selection of a low sticking coefficient. In this case, we used a sticking coefficient of 10⁻⁹ which
273 is lower than most sticking coefficient values reported previously for metal ALD^{3,78}. With higher
274 sticking coefficients of the order of 10⁻⁶, and 10⁻³, a step-like saturation profile was seen, with an
275 abrupt adsorption front (supporting information Figure S9). The low sticking coefficient may be
276 linked to the nucleation delay reported for MePtCpMe₃/O₂ in earlier studies⁷⁹⁻⁸¹. Also, the ALD



277 temperature in our study, 110 °C, which was lower than that reported in most of the literature for Pt
278 ALD on particulate materials, which typically used ~ 300 °C)^{30,75–77,82,83} and the low temperature
279 may be linked to the low sticking coefficient. As shown previously,^{74,84} using a low deposition
280 temperature is possible because operating at atmospheric pressure allows a higher partial pressure
281 of O₂, enabling the process to proceed at a lower temperature. This temperature was chosen for
282 the ALD process because lower process temperatures typically lead to a narrower particle size
283 distribution and more stable Pt catalysts⁷⁴.

284 4.3 Pt particle size

285 With increasing ALD exposure time of MeCpMePt₃, there was an increase in Pt crystallite size and
286 a decrease in dispersion seen from the CO chemisorption results (Table 4). The increase in particle
287 size may be related to a slow increase of Pt uptake with longer exposure time (Table S2 in the
288 supporting information)^{79,85}. This increasing Pt particle size might also be explained by Ostwald
289 particle ripening phenomena⁸⁶ and/or island aggregation⁸⁷. Coalescence-driven growth of Pt has
290 been reported elsewhere, where particle size evolution was largely governed by surface migration
291 and diffusion-driven coalescence rather than precursor adsorption alone^{79,88}.

292 4.4 Comparison to state of the art mesoporous particle coating by ALD

293 The results of this work seem to indicate that the platinum reactant does not thermally decompose
294 at the used ALD reaction temperature (110 °C). It was previously shown through Monte Carlo
295 simulations³ that for processes that in addition to ideal ALD include a continuous CVD-type de-
296 composition component, thermal decomposition would be expected to manifest itself through a
297 higher platinum content in the outer areas of the particles. The absence of such a concentration
298 gradient points to the absence of thermal decomposition.

299 In this work, a uniform Pt distribution was obtained for porous spheres with an AR of 126,000:1
300 (AR, taken as the ratio of the particle radius to the pore diameter). Previously, to the authors'
301 knowledge on porous spheres (see Table 1), the highest previously reported AR was 43,103:1⁴⁸
302 for which a uniform distribution by noble metal ALD (Ru(EtCp₂)/O₂ process) was seen. For Pt,
303 uniform coating on mesoporous silica gel particles (size: 30–75 μm) was shown up to an AR of



304 6,250:1 using a MeCpPtMe₃/O₂ process in a fluidized bed reactor operated at vacuum conditions⁵⁹.
305 In the case of a Pd(Hfac₂)/formalin process on porous alumina spheres with extremely high aspect
306 ratios (~125,000 :1), only a thin egg-shell type coating was demonstrated⁴⁶.

307 Other studies have also demonstrated uniform distribution in porous high aspect ratio materials
308 with different shapes than spheres. On silica aerogel monolith slabs, the penetration depth increased
309 with increasing exposure time and uniform coating was seen for AR 60,000:1^{89,90}. On mesoporous
310 alumina (size: 125-300 μm) with AR up to 12,500:1, a TiO₂ overcoat extending through the alu-
311 mina support was observed (Ti[OCH(CH₃)₂]₄/H₂O process) with some additional titanium around
312 the edges of the particles⁹¹, which may suggest the presence of some CVD type decomposition in
313 addition to ALD³.

314 In conclusion, while uniform ALD coatings on mesoporous supports have been previously re-
315 ported before under specific ALD process conditions, the present work extends such uniformity to
316 significantly higher aspect ratios, ca. 125,000:1.

317 5 Conclusion

318 In this work, ALD of Pt on mesoporous alumina spheres was shown using (methylcyclopentadi-
319 enyl)trimethyl platinum [MeCpPtMe₃] and synthetic air at 110 °C in a fluidized bed reactor oper-
320 ated at atmospheric pressure. Macroscopic distribution of platinum, analyzed by LEIS, varied from
321 egg-shell to uniform, depending on the exposure time. Uniform distribution could be obtained even
322 on spheres of 2.5 mm diameter, with an aspect ratio of ca. 125,000:1 (ratio of particle radius to
323 average pore diameter). For the longest exposure time (2880 s) and five ALD cycles, a Pt weight
324 loading on the order of 3.5 to 4 wt% was obtained, giving an average GPC, expressed as average
325 areal number density, of 0.14 to 0.12 Pt atoms/nm².

326 A diffusion–reaction model for porous spheres⁵⁶ was used to simulate Pt distribution. In order
327 to make the modeling results resemble the experimental results, a very low sticking coefficient
328 (on the order of 10⁻⁹) had to be assumed. This is likely in line with the strong nucleation delay
329 observed for this process. The diffusion–reaction simulations, based on the ideal ALD assumption
330 (i.e., saturating, irreversible reactions) were able to reproduce the main features of the process.



331 **6 Acknowledgments**

332 The authors thank Dirk Niemeyer (SASOL Ltd.) for providing the alumina supports. C.G. thanks
333 Reetta Karinen for fruitful discussions and feedback. This work was financially supported by the
334 Research Council of Finland (former Academy of Finland) ALDI consortium, decision no. 331082;
335 by the Vilho, Yrjö and Kalle Väisälä Foundation of the Finnish Academy of Science and Letters;
336 by the Business Finland project Forest CUMP (Dnro 2158/31/2022); and by the Business Finland
337 project e-Fuel (Dnro 43287/31/2020). C.G. thanks the Walter Ahlström foundation for an encour-
338 agement grant. Computational resources were provided by the Aalto Science-IT services, and CSC
339 – IT Center for Science, Finland.

340 **7 Conflicts of interest**

341 There are no conflicts of interest to declare.

342 **8 Data availability**

343 Data will be made available on reasonable request. The simulation code used for the diffusion–reaction
344 model of porous spheres will be made publicly available as open research software on GitHub
345 (https://github.com/Aalto-Puurunen/ALD_porous-sphere_JV).

346 **9 Author contributions**

347 Christine Gonsalves: Data Curation, Formal analysis, Investigation, Methodology, Validation,
348 Visualization, Writing-original draft, Writing-review and editing. Jānis Jārvilehto: Conceptual-
349 ization, Data Curation, Formal analysis, Investigation, Methodology, Validation, Visualization,
350 Writing-original draft, Writing-review and editing. Saeed Saedy: Conceptualization, Data Cura-
351 tion, Investigation, Methodology, Validation, Writing-review and editing. Jorge A. Velasco: Inves-
352 tigation, Methodology, Software, Supervision, Writing-original draft, Writing-review and editing.
353 Philipp Brūner: Data Curation, Investigation, Visualization, Writing-original draft, Writing-review
354 and editing. Thomas Grehl: Data Curation, Supervision. Niko Heikkinen: Investigation, Software,



355 Validation. Juha Lehtonen: Software, Supervision. Ruud van Ommen: Conceptualization, Method-
356 ology, Resources, Supervision, Writing-review and editing. Riikka Puurunen: Conceptualization,
357 Funding acquisition, Methodology, Project administration, Resources, Supervision, Writing-review
358 and editing.

359 List of symbols

360	c	Sticking coefficient (-)
361	c_M	Areal number density (nm^{-2})
362	D_A	Molecular diffusion coefficient ($\text{m}^2 \text{s}^{-1}$)
363	D_{eff}	Effective diffusion coefficient ($\text{m}^2 \text{s}^{-1}$)
364	D_{Kn}	Knudsen diffusion coefficient ($\text{m}^2 \text{s}^{-1}$)
365	d_A	Hard-sphere diameter of molecule A (m)
366	d_I	Hard-sphere diameter of the inert gas molecule (m)
367	d_{pore}	Pore diameter of the support (m)
368	ε	Porosity (-)
369	ϕ_{coat}	Coated volume fraction (V_d/V_R) of the porous sphere (-)
370	Kn	Knudsen number
371	m_s	Mass of the support (g)
372	m_t	Total mass of the sample (g)
373	M_M	Molar mass of the metal (g mol^{-1})
374	M_A	Molar mass of reactant A (kg mol^{-1})
375	M_I	Molar mass of inert gas I (kg mol^{-1})
376	n	Stoichiometric factor (number of CO molecules adsorbed per surface metal atom) (-)
377	n_A	Volumetric reactant A number density (m^{-3})
378	N_0	Avogadro's constant (mol^{-1})
379	P_d	Desorption probability (s^{-1})
380	q	Adsorption capacity of metal M atoms in the ALD growth of film of the M_yZ_x material
381		(nm^{-2}) (i.e., GPC expressed as areal number density)
382	ρ_s	Skeletal density of the support, here γ -alumina 3.6 g cm^{-3} ⁶⁹



383	S	Specific surface area of the support ($\text{m}^2 \text{g}^{-1}$)
384	\bar{s}	Ratio of surface area (S) and pore volume (V_{pore})
385	τ	Tortuosity (-)
386	θ	Surface coverage (-)
387	t	Time (s)
388	T	Temperature (K)
389	\bar{v}_A	Thermal velocity of molecule A (m s^{-1})
390	V_d	Coated volume of the sphere ($\text{cm}^3 \text{g}^{-1}$)
391	V_{pore}	Pore volume ($\text{cm}^3 \text{g}^{-1}$)
392	V_R	Total volume of a sphere ($\text{cm}^3 \text{g}^{-1}$)
393	w_M	Weight fraction of the metal (%)



394 **References**

- 395 [1] J. R. van Ommen, A. Goulas and R. L. Puurunen, in *Kirk-Othmer Encyclopedia of Chemical*
396 *Technology*, John Wiley & Sons, Ltd, 2021, pp. 1–42.
- 397 [2] R. L. Puurunen, Surface chemistry of atomic layer deposition: A case study for the trimethy-
398 laluminum/water process, *Journal of Applied Physics*, 2005, **97**, 121301.
- 399 [3] V. Cremers, R. L. Puurunen and J. Dendooven, Conformality in atomic layer deposition:
400 Current status overview of analysis and modelling, *Applied Physics Reviews*, 2019, **6**, 021302.
- 401 [4] V. Miikkulainen, M. Leskelä, M. Ritala and R. L. Puurunen, Crystallinity of inorganic films
402 grown by atomic layer deposition: Overview and general trends, *Journal of Applied Physics*,
403 2013, **113**, 021301.
- 404 [5] G. Popov, M. Mattinen, A. Vihervaara and M. Leskelä, Recent trends in thermal atomic layer
405 deposition chemistry, *Journal of Vacuum Science & Technology A*, 2025, **43**, 030801.
- 406 [6] C. Detavernier, J. Dendooven, S. P. Sree, K. F. Ludwig and J. A. Martens, Tailoring
407 nanoporous materials by atomic layer deposition, *Chemical Society Reviews*, 2011, **40**, 5242–
408 5253.
- 409 [7] J. R. van Ommen and A. Goulas, Atomic layer deposition on particulate materials, *Materials*
410 *Today Chemistry*, 2019, **14**, 100183.
- 411 [8] J. Yim, E. Haimi, M. Mäntymäki, V. Kärkäs, R. Bes, A. A. Gutierrez, K. Meinander, P. Brüner,
412 T. Grehl, L. Gell, T. Viinikainen, K. Honkala, S. Huotari, R. Karinen, M. Putkonen and R. L.
413 Puurunen, Atomic Layer Deposition of Zinc Oxide on Mesoporous Zirconia Using Zinc(II)
414 Acetylacetonate and Air, *Chemistry of Materials*, 2023, **35**, 7915–7930.
- 415 [9] B. J. O'Neill, D. H. K. Jackson, J. Lee, C. Canlas, P. C. Stair, C. L. Marshall, J. W. Elam, T. F.
416 Kuech, J. A. Dumesic and G. W. Huber, Catalyst Design with Atomic Layer Deposition, *Acs*
417 *Catalysis*, 2015, **5**, 1804–1825.
- 418 [10] A. Arandia, J. A. Velasco, A. Sajid, J. Yim, H. Shamshad, H. Jiang, A. Chahal, A. K. Singh,
419 C. Gonsalves, R. Karinen and R. L. Puurunen, Atomic layer deposited zinc promoted cop-



- 420 per catalysts for carbon dioxide hydrogenation to methanol: Influence of support, *Catalysis*
421 *Today*, 2025, **454**, 115283.
- 422 [11] Y. Koshtyal, D. Olkhovskii, A. Rumyantsev and M. Maximov, Applications and Advantages
423 of Atomic Layer Deposition for Lithium-Ion Batteries Cathodes: Review, *Batteries*, 2022, **8**,
424 184.
- 425 [12] R. Saleh, A. Memarzadeh, D. Hurdoganoglu, S. Sahmani, T.-C. Jen and B. Safaei, A compre-
426 hensive review on atomic layer deposition on key components in fuel cells, *Fuel*, 2025, **395**,
427 135172.
- 428 [13] R. Verstraete, G. Rampelberg, H. Rijckaert, I. Van Driessche, E. Coetsee, M.-M. Duvenhage,
429 P. F. Smet, C. Detavernier, H. Swart and D. Poelman, Stabilizing fluoride phosphors: surface
430 modification by atomic layer deposition, *Chemistry of Materials*, 2019, **31**, 7192–7202.
- 431 [14] Z. Zhou, N. Zhou, X. Lu, M. Ten Kate, D. Valdesueiro, J. R. Van Ommen and H. B. Hintzen,
432 Performance improvement by alumina coatings on Y3Al5O12: Ce³⁺ phosphor powder de-
433 posited using atomic layer deposition in a fluidized bed reactor, *Rsc Advances*, 2016, **6**,
434 76454–76462.
- 435 [15] F. Zhang, K. Wu, D. La Zara, F. Sun, M. J. Quayle, G. Petersson, S. Folestad, J. W. Chew
436 and J. R. Van Ommen, Tailoring the flow properties of inhaled micronized drug powders by
437 atomic and molecular layer deposition, *Chemical Engineering Journal*, 2023, **462**, 142131.
- 438 [16] P. M. Piechulla, M. Chen, A. Goulas, R. L. Puurunen and J. R. van Ommen, Atomic layer
439 deposition on particulate materials from 1988 through 2023: A quantitative review of tech-
440 nologies, materials, and applications, *Chemistry of Materials*, 2025, **38**, 20–86.
- 441 [17] A. Goulas and J. R. van Ommen, Scalable production of nanostructured particles using atomic
442 layer deposition, *Kona Powder and Particle Journal*, 2014, **31**, 234–246.
- 443 [18] X. Ren, Q. Lv, L. Liu, B. Liu, Y. Wang, A. Liu and G. Wu, Current progress of Pt and Pt-based
444 electrocatalysts used for fuel cells, *Sustainable Energy & Fuels*, 2020, **4**, 15–30.
- 445 [19] R. J. Spiegel, Platinum and fuel cells, *Transportation Research Part D: Transport and Envi-*
446 *ronment*, 2004, **9**, 357–371.



- 447 [20] O. T. Holton and J. W. Stevenson, The role of platinum in proton exchange membrane fuel
448 cells, *Platinum Metals Review*, 2013, **57**, 259–271.
- 449 [21] P. Rylander, *Catalytic hydrogenation over platinum metals*, Elsevier, 2012.
- 450 [22] S. Yang, J. Kim, Y. J. Tak, A. Soon and H. Lee, Single-Atom Catalyst of Platinum Supported
451 on Titanium Nitride for Selective Electrochemical Reactions, *Angewandte Chemie Interna-*
452 *tional Edition*, 2016, **55**, 2058–2062.
- 453 [23] G. Pardon, H. K. Gatty, G. Stemme, W. v. d. Wijngaart and N. Roxhed, Pt–Al₂O₃ dual layer
454 atomic layer deposition coating in high aspect ratio nanopores, *Nanotechnology*, 2012, **24**,
455 015602.
- 456 [24] A. Vaish, S. Krueger, M. Dimitriou, C. Majkrzak, D. J. Vanderah, L. Chen and K. Gawrisch,
457 Enhancing the platinum atomic layer deposition infiltration depth inside anodic alumina
458 nanoporous membrane, *Journal of Vacuum Science & Technology A*, 2014, **33**, 01A148.
- 459 [25] D. Gu, H. Baumgart, K. Tapily, P. Shrestha, G. Namkoong, X. Ao and F. Müller, Precise
460 control of highly ordered arrays of nested semiconductor/metal nanotubes, *Nano Research*,
461 2011, **4**, 164–170.
- 462 [26] F. Bíró, C. Dücső, G. Z. Radnóczy, Z. Baji, M. Takács and I. Bársony, ALD nano-catalyst
463 for micro-calorimetric detection of hydrocarbons, *Sensors and Actuators B: Chemical*, 2017,
464 **247**, 617–625.
- 465 [27] S. Galbiati, A. Morin and N. Pauc, Supportless Platinum Nanotubes Array by Atomic Layer
466 Deposition as PEM Fuel Cell Electrode, *Electrochimica Acta*, 2014, **125**, 107–116.
- 467 [28] J. Zhang, W. Yu, D. Feng, H. Xu and Y. Qin, Porous titania nanotube confined ultrafine
468 platinum catalysts synthesized by atomic layer deposition with enhanced hydrolytic dehydro-
469 genation performance, *Applied Catalysis B: Environmental*, 2022, **312**, 121405.
- 470 [29] J. Zhang, Z. Yu, Z. Gao, H. Ge, S. Zhao, C. Chen, S. Chen, X. Tong, M. Wang, Z. Zheng
471 and Y. Qin, Porous TiO₂ nanotubes with spatially separated platinum and CoO_x cocatalysts
472 produced by atomic layer deposition for photocatalytic hydrogen production, *Angewandte*
473 *Chemie International Edition*, 2017, **56**, 816–820.



- 474 [30] X. Liang and C. Jiang, Atomic layer deposited highly dispersed platinum nanoparticles sup-
475 ported on non-functionalized multiwalled carbon nanotubes for the hydrogenation of xylose
476 to xylitol, *Journal of Nanoparticle Research*, 2013, **15**, 1890.
- 477 [31] I. J. M. Erkens, M. A. Verheijen, H. C. M. Knoop, W. Keuning, F. Roozeboom and W. M. M.
478 Kessels, Plasma-assisted atomic layer deposition of conformal Pt films in high aspect ratio
479 trenches, *The Journal of Chemical Physics*, 2016, **146**, 052818.
- 480 [32] Y. Zhu, K. A. Dunn and A. E. Kaloyeros, Properties of ultrathin platinum deposited by atomic
481 layer deposition for nanoscale copper-metallization schemes, *Journal of Materials Research*,
482 2007, **22**, 1292–1298.
- 483 [33] D. J. Hagen, J. Yoon, H. Zhang, B. Kalkofen, M. Silinskas, F. Börrnert, H. Han and S. S. P.
484 Parkin, Atomic Layer Deposition of the Conductive Delafossite PtCoO₂, *Advanced Materials*
485 *Interfaces*, 2022, **9**, 2200013.
- 486 [34] S.-M. Han, D. K. Nandi, Y.-H. Joo, T. Shigetomi, K. Suzuki, S. Nabeya, R. Harada and S.-
487 H. Kim, Atomic layer deposition of high-quality Pt thin film as an alternative interconnect
488 replacing Cu, *Journal of Vacuum Science & Technology A*, 2020, **38**, 032404.
- 489 [35] J. Hämäläinen, E. Puukilainen, T. Sajavaara, M. Ritala and M. Leskelä, Low temperature
490 atomic layer deposition of noble metals using ozone and molecular hydrogen as reactants,
491 *Thin Solid Films*, 2013, **531**, 243–250.
- 492 [36] J. Lee, J. Yoon, H. G. Kim, S. Kang, W.-S. Oh, H. Algadi, S. Al-Sayari, B. Shong, S.-H. Kim,
493 H. Kim, T. Lee and H.-B.-R. Lee, Highly conductive and flexible fiber for textile electronics
494 obtained by extremely low-temperature atomic layer deposition of Pt, *NPG Asia Materials*,
495 2016, **8**, e331–e331.
- 496 [37] W.-J. Lee, Z. Wan, C.-M. Kim, I.-K. Oh, R. Harada, K. Suzuki, E.-A. Choi and S.-H.
497 Kwon, Atomic Layer Deposition of Pt Thin Films Using Dimethyl (N,N-Dimethyl-3-Butene-
498 1-Amine-N) Platinum and O₂ Reactant, *Chemistry of Materials*, 2019, **31**, 5056–5064.
- 499 [38] Y. Son, S. B. Kim, D. Mohapatra, T. Cheon and S.-H. Kim, Advanced Atomic Layer Modula-



- 500 tion Based Highly Homogeneous PtRu Precious Metals Alloy Thin Films, *Advanced Science*,
501 2025, e03561.
- 502 [39] T. Aaltonen, A. Rahtu, M. Ritala and M. Leskelä, Reaction mechanism studies on atomic
503 layer deposition of ruthenium and platinum, *Electrochemical and solid state letters*, 2003, **6**,
504 C130–C133.
- 505 [40] H. Van Bui, F. Grillo, D. M. Nguyen, M. D. Dang, A. A. Aarnink, R. A. Wolters, J. R. van
506 Ommen and A. Y. Kovalgin, Highly Reactive Atomic Hydrogen as an Alternative Reactant for
507 Atomic Layer Deposition of Platinum Using MeCpPtMe₃, *The Journal of Physical Chemistry*
508 *C*, 2025.
- 509 [41] S. Kwon and B. Shong, Chemical mechanism for nucleation enhancement in atomic layer
510 deposition of Pt by surface functionalization, *Journal of Vacuum Science & Technology A*,
511 2025, **43**, 012401.
- 512 [42] L.-A. T. Le, H. T. Ta, H. V. Bui and N. L. Nguyen, Atomic Layer Deposition of Platinum on
513 the Oxygen-Pretreated Graphene Surface, *The Journal of Physical Chemistry C*, 2024, **129**,
514 705–714.
- 515 [43] H.-E. Nieminen, M. Putkonen and M. Ritala, In vacuo studies on reaction mechanisms in ALD
516 processes of ruthenium and platinum films, *Applied Surface Science*, 2024, **648**, 159015.
- 517 [44] N. Heikkinen, J. Lehtonen, L. Keskiaväli, J. Yim, S. Shetty, Y. Ge, M. Reinikainen and
518 M. Putkonen, Modelling atomic layer deposition overcoating formation on a porous hetero-
519 geneous catalyst, *Physical Chemistry Chemical Physics*, 2022, **24**, 20506–20516.
- 520 [45] S. W. Han, D. H. Kim, M.-G. Jeong, K. J. Park and Y. D. Kim, CO oxidation catalyzed by
521 NiO supported on mesoporous Al₂O₃ at room temperature, *Chemical Engineering Journal*,
522 2016, **283**, 992–998.
- 523 [46] A. C. Bueno, M. Mayer, M. Weber, M. Bechelany, M. Klotz and D. Farrusseng, Impregnation
524 Protocols on Alumina Beads for Controlling the Preparation of Supported Metal Catalysts,
525 *Catalysts*, 2019, **9**, 577.



- 526 [47] J. W. Elam, J. A. Libera, T. H. Huynh, H. Feng and M. J. Pellin, Atomic Layer Deposition of
527 Aluminum Oxide in Mesoporous Silica Gel, *The Journal of Physical Chemistry C*, 2010, **114**,
528 17286–17292.
- 529 [48] I. H. Kim, M.-G. Jeong, S. W. Han, E. J. Park, Y. K. Hwang and Y. D. Kim, CO oxidation
530 catalyzed by RuO₂ nanoparticles supported on mesoporous Al₂O₃ prepared via atomic layer
531 deposition, *Current Applied Physics*, 2016, **16**, 1407–1412.
- 532 [49] G. Ballai, T. Kotnik, M. Finšgar, A. Pintar, Z. Kónya, A. Sági and S. Kovačič, Highly Porous
533 Polymer Beads Coated with Nanometer-Thick Metal Oxide Films for Photocatalytic Oxida-
534 tion of Bisphenol A, *ACS Applied Nano Materials*, 2023, **6**, 20089–20098.
- 535 [50] R. G. Gordon, D. Hausmann, E. Kim and J. Shepard, A Kinetic Model for Step Coverage by
536 Atomic Layer Deposition in Narrow Holes or Trenches, *Chemical Vapor Deposition*, 2003, **9**,
537 73–78.
- 538 [51] M. Ylilammi, O. M. E. Ylivaara and R. L. Puurunen, Modeling growth kinetics of thin films
539 made by atomic layer deposition in lateral high-aspect-ratio structures, *Journal of Applied*
540 *Physics*, 2018, **123**, 205301.
- 541 [52] J. Yim, E. Verkama, J. A. Velasco, K. Arts and R. L. Puurunen, Conformality of atomic layer
542 deposition in microchannels: impact of process parameters on the simulated thickness profile,
543 *Physical Chemistry Chemical Physics*, 2022, **24**, 8645–8660.
- 544 [53] J. Järvillehto, J. A. Velasco, J. Yim, C. Gonsalves and R. L. Puurunen, Simulation of con-
545 formality of ALD growth inside lateral channels: comparison between a diffusion–reaction
546 model and a ballistic transport–reaction model, *Physical Chemistry Chemical Physics*, 2023,
547 **25**, 22952–22964.
- 548 [54] C. Gonsalves, J. A. Velasco, J. Yim, J. Järvillehto, V. Vuorinen and R. L. Puurunen, Simulated
549 conformality of atomic layer deposition in lateral channels: the impact of the Knudsen num-
550 ber on the saturation profile characteristics, *Physical Chemistry Chemical Physics*, 2024, **26**,
551 28431–28448.



- 552 [55] R. A. Adomaitis, A Ballistic Transport and Surface Reaction Model for Simulating Atomic
553 Layer Deposition Processes in High-Aspect-Ratio Nanopores, *Chemical Vapor Deposition*,
554 2011, **17**, 353–365.
- 555 [56] N. Heikkinen, J. Lehtonen and R. L. Puurunen, An atomic layer deposition diffusion–reaction
556 model for porous media with different particle geometries, *Physical Chemistry Chemical*
557 *Physics*, 2024, **26**, 7580–7591.
- 558 [57] N. Heikkinen, *Doctoral thesis*, Aalto University, 2025.
- 559 [58] J. Libera, J. Elam and M. Pellin, Conformal ZnO coatings on high surface area silica gel using
560 atomic layer deposition, *Thin Solid Films*, 2008, **516**, 6158–6166.
- 561 [59] J. Li, X. Liang, D. M. King, Y.-B. Jiang and A. W. Weimer, Highly dispersed Pt nanoparticle
562 catalyst prepared by atomic layer deposition, *Applied Catalysis B: Environmental*, 2010, **97**,
563 220–226.
- 564 [60] F. Grillo, H. Van Bui, D. La Zara, A. A. Aarnink, A. Y. Kovalgin, P. Kooyman, M. T. Kreutzer
565 and J. R. van Ommen, From single atoms to nanoparticles: Autocatalysis and metal aggrega-
566 tion in atomic layer deposition of Pt on TiO₂ nanopowder, *Small*, 2018, **14**, 1800765.
- 567 [61] A. Goulas and J. Ruud Van Ommen, Atomic layer deposition of platinum clusters on titania
568 nanoparticles at atmospheric pressure, *Journal of Materials Chemistry A*, 2013, **1**, 4647.
- 569 [62] D. Valdesueiro, G. M. Meesters, M. T. Kreutzer and J. R. Van Ommen, Gas-phase deposition
570 of ultrathin aluminium oxide films on nanoparticles at ambient conditions, *Materials*, 2015,
571 **8**, 1249–1263.
- 572 [63] F. Grillo, M. T. Kreutzer and J. R. van Ommen, Modeling the precursor utilization in atomic
573 layer deposition on nanostructured materials in fluidized bed reactors, *Chemical Engineering*
574 *Journal*, 2015, **268**, 384–398.
- 575 [64] S. Brunauer, P. H. Emmett and E. Teller, Adsorption of gases in multimolecular layers, *Journal*
576 *of the American chemical society*, 1938, **60**, 309–319.



- 577 [65] B. C. Lippens, B. G. Linsen and J. H. d. Boer, Studies on pore systems in catalysts I. The
578 adsorption of nitrogen; apparatus and calculation, *Journal of Catalysis*, 1964, **3**, 32–37.
- 579 [66] J. A. Velasco and R. L. Puurunen, *Diffusion-reaction model for ALD on porous*
580 *spheres*[*GitHub Repository*], [https://github.com/Aalto-Puurunen/ALD_](https://github.com/Aalto-Puurunen/ALD_porous-sphere_JV)
581 [porous-sphere_JV](https://github.com/Aalto-Puurunen/ALD_porous-sphere_JV), 2025.
- 582 [67] R. Evans III, G. Watson and E. Mason, Gaseous diffusion in porous media at uniform pressure,
583 *The journal of chemical physics*, 1961, **35**, 2076–2083.
- 584 [68] C. H. Bartholomew and R. J. Farrauto, *Catalyst Materials, Properties and Preparation*, John
585 Wiley & Sons, Inc., 2nd edn., 2005, pp. 60–117.
- 586 [69] H. Hashimoto, Y. Onodera, S. Tahara, S. Kohara, K. Yazawa, H. Segawa, M. Murakami and
587 K. Ohara, Structure of alumina glass, *Scientific Reports*, 2022, **12**, 516.
- 588 [70] J. Beeckman, Mathematical description of heterogeneous materials, *Chemical engineering*
589 *science*, 1990, **45**, 2603–2610.
- 590 [71] L. Shen and Z. Chen, Critical review of the impact of tortuosity on diffusion, *Chemical Engi-*
591 *neering Science*, 2007, **62**, 3748–3755.
- 592 [72] J. Dendooven, *Atomically-Precise Methods for Synthesis of Solid Catalysts*, Royal Society of
593 Chemistry, Cambridge, UK, 2014, vol. 22.
- 594 [73] R. L. Puurunen, Growth per cycle in atomic layer deposition: a theoretical model, *Chemical*
595 *Vapor Deposition*, 2003, **9**, 249–257.
- 596 [74] H. Van Bui, F. Grillo, S. S. Kulkarni, R. Bevaart, N. Van Thang, B. Van Der Linden, J. A.
597 Moulijn, M. Makkee, M. T. Kreutzer and J. R. Van Ommen, Low-temperature atomic layer
598 deposition delivers more active and stable Pt-based catalysts, *Nanoscale*, 2017, **9**, 10802–
599 10810.
- 600 [75] W.-J. Lee and S.-H. Kwon, Role of Acid Treatment of the Carbon Support in the Growth of
601 Atomic-Layer-Deposited Pt Nanoparticles for PEMFC Fabrication, *Particle & Particle Sys-*
602 *tems Characterization*, 2023, **40**, 2200158.



- 603 [76] C. Jiang and X. Liang, Catalytic hydrogen transfer of ketones over atomic layer deposited
604 highly-dispersed platinum nanoparticles supported on multi-walled carbon nanotubes, *Catal-*
605 *ysis Communications*, 2014, **46**, 41–45.
- 606 [77] A. M. Lubers, C. L. Muhich, K. M. Anderson and A. W. Weimer, Mechanistic studies for
607 depositing highly dispersed Pt nanoparticles on carbon by use of trimethyl (methylcyclopentadienyl) platinum (IV) reactions with O₂ and H₂, *Journal of Nanoparticle Research*, 2015,
608 **17**, 179.
- 610 [78] J. Yim, O. M. Ylivaara, M. Ylilammi, V. Korpelainen, E. Haimi, E. Verkama, M. Utriainen and
611 R. L. Puurunen, Saturation profile based conformality analysis for atomic layer deposition:
612 aluminum oxide in lateral high-aspect-ratio channels, *Physical Chemistry Chemical Physics*,
613 2020, **22**, 23107–23120.
- 614 [79] J. Dendooven, M. Van Daele, E. Solano, R. K. Ramachandran, M. M. Minjauw, A. Resta,
615 A. Vlad, Y. Garreau, A. Coati, G. Portale *et al.*, Surface mobility and impact of precursor
616 dosing during atomic layer deposition of platinum: in situ monitoring of nucleation and island
617 growth, *Physical Chemistry Chemical Physics*, 2020, **22**, 24917–24933.
- 618 [80] J. Dendooven, R. K. Ramachandran, K. Devloo-Casier, G. Rampelberg, M. Filez, H. Poelman,
619 G. B. Marin, E. Fonda and C. Detavernier, Low-temperature atomic layer deposition of plat-
620 inum using (methylcyclopentadienyl) trimethylplatinum and ozone, *The Journal of Physical*
621 *Chemistry C*, 2013, **117**, 20557–20561.
- 622 [81] P. Shrestha, D. Gu, N. Tran, K. Tapily, H. Baumgart and G. Namkoong, Investigation of
623 Volmer-Weber growth during the nucleation phase of ALD platinum thin films and template
624 based platinum nanotubes, *ECS Transactions*, 2010, **33**, 127.
- 625 [82] J. Li, B. Zhang, Y. Chen, J. Zhang, H. Yang, J. Zhang, X. Lu, G. Li and Y. Qin, Styrene
626 hydrogenation performance of Pt nanoparticles with controlled size prepared by atomic layer
627 deposition, *Catalysis Science & Technology*, 2015, **5**, 4218–4223.
- 628 [83] A. Lubers, A. Drake, D. Ludlow and A. Weimer, Electrochemical hydrogen pumping using



- 629 a platinum catalyst made in a fluidized bed via atomic layer deposition, *Powder Technology*,
630 2016, **296**, 72–78.
- 631 [84] H. Van Bui, A. P. Nguyen, M. D. Dang, T. D. Dinh, P. J. Kooyman and J. R. Van Ommen, What
632 could be the low-temperature limit of atomic layer deposition of platinum using MeCpPtMe
633 3 and oxygen?, *Chemical Communications*, 2024, **60**, 14045–14048.
- 634 [85] X. Liang, Y. Zhou, J. Li and A. W. Weimer, Reaction mechanism studies for platinum nanopar-
635 ticle growth by atomic layer deposition, *Journal of Nanoparticle Research*, 2011, **13**, 3781–
636 3788.
- 637 [86] A. J. Mackus, M. A. Verheijen, N. Leick, A. A. Bol and W. M. Kessels, Influence of oxy-
638 gen exposure on the nucleation of platinum atomic layer deposition: consequences for film
639 growth, nanopatterning, and nanoparticle synthesis, *Chemistry of Materials*, 2013, **25**, 1905–
640 1911.
- 641 [87] F. Grillo, H. Van Bui, J. A. Moulijn, M. T. Kreutzer and J. R. Van Ommen, Understanding
642 and controlling the aggregative growth of platinum nanoparticles in atomic layer deposition:
643 An avenue to size selection, *The journal of physical chemistry letters*, 2017, **8**, 975–983.
- 644 [88] S. M. Geyer, R. Methaapanon, R. Johnson, S. Brennan, M. F. Toney, B. Clemens and S. Bent,
645 Structural evolution of platinum thin films grown by atomic layer deposition, *Journal of Ap-
646 plied Physics*, 2014, **116**, 064905.
- 647 [89] A. J. Gayle, Z. J. Berquist, Y. Chen, A. J. Hill, J. Y. Hoffman, A. R. Bielinski, A. Lenert
648 and N. P. Dasgupta, Tunable atomic layer deposition into ultra-high-aspect-ratio (> 60000: 1)
649 aerogel monoliths enabled by transport modeling, *Chemistry of Materials*, 2021, **33**, 5572–
650 5583.
- 651 [90] V. A. Vogt, A. J. Gayle, A. Miranda Mañón, A. Lenert and N. P. Dasgupta, Modeling diffusion
652 and depletion in high-aspect-ratio atomic layer deposition processes: Process parameters and
653 manufacturing impacts, *Journal of Vacuum Science & Technology A*, 2025, **43**, 062401.
- 654 [91] J. A. Moulijn, J. R. van Ommen, A. Goulas, D. Valdesueiro, J. Juan-Alcañiz, K.-M. Au-
655 Yeung, L. Woning and J. A. Bergwerff, Synthesis of highly-uniform titania overcoats on a



656 mesoporous alumina catalyst support by atomic layer deposition and their application in hy-
657 droprocessing, *Catalysis Science & Technology*, 2023, **13**, 3537–3544.



Data Availability Statement

View Article Online
DOI: 10.1039/D5LF00395D

The simulation code used for the diffusion–reaction model of porous spheres will be made publicly available as open research software on GitHub (https://github.com/Aalto-Puurunen/ALD_porous-sphere_JV). Data will be made available upon reasonable request.

